


## Article

# Pyrolysis of Biomass Pineapple Residue and Banana Pseudo-Stem: Kinetics, Mechanism and Valorization of Bio-Char

Xin Wang <sup>1,\*</sup> , Shuo Yang <sup>1</sup>, Boxiong Shen <sup>2,\*</sup>, Jiancheng Yang <sup>1</sup>  and Lianfei Xu <sup>1</sup>

<sup>1</sup> Tianjin Key Laboratory of Clean Energy and Pollution Control, School of Energy and Environmental Engineering, Hebei University of Technology, Tianjin 300401, China; yangshuonh@126.com (S.Y.); yangjch1023@hebut.edu.cn (J.Y.); xulianfei2006@126.com (L.X.)

<sup>2</sup> School of Chemical Engineering, Hebei University of Technology, Tianjin 300401, China

\* Correspondence: wangxinh@hebut.edu.cn (X.W.); shenbx@hebut.edu.cn (B.S.); Tel.: +86-022-60435279 (X.W.); Fax: +86-022-60435279 (X.W.)

**Abstract:** Pineapple residue and banana pseudo-stem are waste from agricultural production in tropical zones, and the characteristics of their pyrolysis should be explored for high-value utilization. Kinetics, thermodynamics, reaction mechanism and valorization of bio-char during pyrolysis of these feedstock were conducted in this study. In biomass mainly decomposed at 150–500 °C, there was a significant mass loss peak for banana pseudo-stem at 650 °C. The activation energy range of pineapple residue and banana pseudo-stem, based on a multi-heating rate method, was 159–335 and 169–364 kJ/mol, respectively. Based on the Gaussian multi-peak fitting method, derivative thermogravimetric curves of pineapple residue and banana pseudo-stem were deconvoluted with three or four fitting peaks, based on the key components in biomass. Interaction between intermediates during pyrolysis increased the complexity of kinetic data. The main carbon number of organic volatiles during pyrolysis was C<sub>4</sub> and C<sub>5</sub> for pineapple residue, and C<sub>2</sub> and C<sub>3</sub> for banana pseudo-stem. The high content of cellulose and hemicellulose in biomass improved the yield of volatiles. Porous carbon sourced from pineapple residue and banana pseudo-stems had specific capacitance of 375 F/g and 297 F/g at a current density of 0.5 A/g, respectively. This suggested pineapple residue and banana pseudo-stem as a potential feedstock for electrochemical materials.

**Keywords:** pineapple residue; banana pseudo-stem; pyrolysis; kinetics; deconvolution; porous carbon; electrochemical property



**Citation:** Wang, X.; Yang, S.; Shen, B.; Yang, J.; Xu, L. Pyrolysis of Biomass Pineapple Residue and Banana Pseudo-Stem: Kinetics, Mechanism and Valorization of Bio-Char. *Catalysts* **2022**, *12*, 840. <https://doi.org/10.3390/catal12080840>

Academic Editor: Keith Hohn

Received: 21 June 2022

Accepted: 27 July 2022

Published: 30 July 2022

**Publisher's Note:** MDPI stays neutral with regard to jurisdictional claims in published maps and institutional affiliations.



**Copyright:** © 2022 by the authors. Licensee MDPI, Basel, Switzerland. This article is an open access article distributed under the terms and conditions of the Creative Commons Attribution (CC BY) license (<https://creativecommons.org/licenses/by/4.0/>).

## 1. Introduction

Pyrolysis is a thermochemical process which converts biomass into bio-oil, bio-char, and gaseous products at 400–600 °C in an oxygen-free environment [1]. A large amount of feedstock has been explored by pyrolysis, such as microalgae, oil crops, agricultural waste, sewage sludge, and municipal solid waste. Tropical agricultural crop waste, including pineapple residue and banana pseudo-stem, had also been evaluated [2,3], and their pyrolysis provides an alternative pathway to realize the recovery of energy and materials. For example, pyrolysis kinetics of pineapple peel was conducted via the Coats and Redfern method, and the diffusion-nucleation mechanism was confirmed for the pyrolysis process [2]. For pyrolysis of banana pseudo-stem by a fluidized bed reactor with a nominal capacity of 300 g/h, the optimum pyrolysis temperature and residence time were 500 °C and 1.02 s, respectively [3]. Recently, related research has mainly focused on optimization of pyrolysis mechanism and valorization of pyrolysis products.

Pyrolysis of biomass is the overlapping thermal decomposition process of their key components (cellulose, hemicellulose, and lignin) and kinetic parameters (activation energy, mechanism equation, and pre-exponential factor), which can be calculated by approaches

such as the multi-step model-fitting method, distributed reactivity method, the isoconversional method, and the deconvolution method [4]. For example, distributed reactivity and isoconversional methods were compared to assess pyrolysis kinetics of pineapple waste, which showed a fluctuating profile of activation energy (150–550 kJ/mol) throughout the entire range of conversion. It was associated with a high extractive content in peel samples [5]. Apparent activation energy for thermal decomposition of pineapple waste (crown and leaves) was 122–259 kJ/mol, which was calculated by the isoconversional method and the result was affected by the ratio of carbon and oxygen in samples [6]. The isoconversional method was also used to determine activation energy (130–192 kJ/mol) of banana pseudo-stem. Its pyrolysis was divided into three stages following a three-dimensional diffusion model [7]. Additionally, catalytic pyrolysis (impregnation of banana pseudo-stem with Ru and Fe) apparently decreased activation energy from 116 kJ/mol to 70–80 kJ/mol [8]. Although pyrolysis kinetics have been well developed in recent years, pyrolysis kinetics of tropical agricultural crop waste is not fully explored, especially the difference between these pyrolysis kinetic methods.

Biomass-based carbon materials can realize valorization of pyrolysis products, especially for tropical agricultural waste. Pineapple residue and banana pseudo-stem can be used to produce porous carbon materials for pollutant removal, CO<sub>2</sub> absorption, and electrochemical application. For example, bio-char derived from pineapple residue exhibited a Cr(VI) adsorption capacity of 41.67 mg/g [9]. A process of freeze-drying followed by pyrolysis was developed for preparing microporous carbon from banana pseudo-stems, and the produced carbon materials exhibited a CO<sub>2</sub> adsorption capacity of 7.1 mmol/g after chemical activation [10]. Recently, activated bio-char was used as electrode materials of supercapacitors, with high surface areas and low production cost [11]. Microporous carbon material with a pore size of 1–2 nm derived from flaxseed residue exhibited excellent electrochemical performance and its specific capacitance was up to 369 F/g in KOH electrolyte [12]. Hierarchical porous carbons derived from Miscanthus grass achieved high micropore volume (0.26 cm<sup>3</sup>/g) and specific capacitance (188 F/g) [13]. Although biomass has been converted into carbon-based materials, the potential of tropical agricultural waste (pineapple residue and banana pseudo-stem) used as electrode materials of supercapacitors by pyrolysis needs further research and evaluation.

In this study, kinetics of pyrolysis was compared by the Friedman method (multi-heating rate method) and deconvolution method (multi-peak fitting method) with biomass pineapple residue and banana pseudo-stem. Evolved gas during pyrolysis was also analyzed through Fourier transform infrared spectroscopy (FTIR) and gas chromatography-mass spectrometry (GC-MS). Pyrolysis mechanism was elucidated based on thermogravimetric analysis (TGA) curves, differential scanning calorimetry (DSC) curves, kinetic/thermodynamic results, and evolved gas analysis. Furthermore, bio-char derived from pineapple residue and banana pseudo-stem was activated by KOH into porous carbon, which was evaluated as electrode materials in order to realize high-value utilization of biomass. This study will provide necessary information for energy recovery and resource utilization of tropical agricultural crop waste.

## 2. Results and Discussion

### 2.1. Thermogravimetric Characteristics during Biomass Pyrolysis

Samples (pineapple residue and banana pseudo-stem) were pyrolyzed to reveal their mass loss characteristics and reaction mechanism during pyrolysis. Proximate analysis and ultimate analysis of biomass waste are shown in Table 1. The volatile content of pineapple residue was 72.12%, which was beneficial to the pyrolysis process and porous structure of bio-char. Ash content of banana pseudo-stem was 23.53%, which might affect pyrolysis reaction rates or change the pyrolysis reaction pathway. The content of nitrogen and sulfur in samples were both low, which reflected the possibility of being an environmentally friendly energy source. Figure 1 shows thermogravimetric (TG) and derivative thermogravimetric (DTG) curves of pineapple residue and banana pseudo-stem

at five heating rates ( $\beta = 5, 10, 15, 20,$  and  $25\text{ }^{\circ}\text{C}/\text{min}$ ) under nitrogen atmosphere. The main decomposition temperature range was  $120\text{--}500\text{ }^{\circ}\text{C}$  for both samples. There was a small mass loss peak at  $600\text{--}700\text{ }^{\circ}\text{C}$  for banana pseudo-stem. It was observed that the temperature corresponding to the maximum mass loss peak of DTG curves increased significantly, and pyrolysis process shifted toward high temperature zone at the increase of heating rates, which could be attributed to the short heating time and hysteresis of pyrolysis reaction [14,15]. Carbonization occurring on biomass surface could also hinder heat transfer and exacerbate thermal hysteresis [16].

**Table 1.** Proximate analysis and ultimate analysis of biomass waste.

Items	Pineapple Residue	Banana Pseudo-Stem
Water (wt. %)	$2.15 \pm 0.01$	$1.93 \pm 0.01$
Ash (wt. %)	$6.24 \pm 0.01$	$23.53 \pm 0.07$
Volatile (wt. %)	$72.12 \pm 0.58$	$59.77 \pm 0.48$
Fixed carbon (wt. %)	$19.50 \pm 0.06$	$14.78 \pm 0.04$
Heating value (MJ/kg)	$17.73 \pm 0.04$	$13.28 \pm 0.03$
C (wt. %) <sup>a</sup>	$44.95 \pm 0.05$	$33.93 \pm 0.03$
H (wt. %) <sup>a</sup>	$5.50 \pm 0.01$	$4.02 \pm 0.01$
O (wt. %) <sup>a</sup>	$47.65 \pm 0.05$	$60.49 \pm 0.06$
N (wt. %) <sup>a</sup>	$1.68 \pm 0.01$	$1.47 \pm 0.01$
S (wt. %) <sup>a</sup>	$0.22 \pm 0.01$	$0.09 \pm 0.01$
Cellulose (wt. %)	$27.35 \pm 1.83$	$17.17 \pm 0.79$
Hemicellulose (wt. %)	$21.15 \pm 0.34$	$8.11 \pm 0.24$
Lignin (wt. %)	$10.25 \pm 0.30$	$35.00 \pm 0.67$

a: results based on water-free and ash-free.

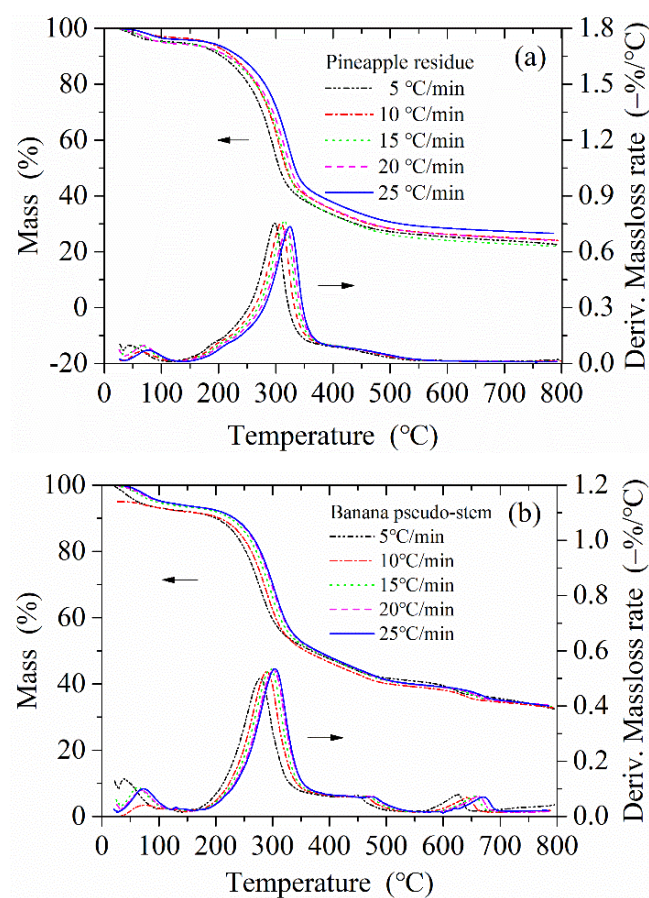


**Figure 1.** TG and DTG curves of (a) pineapple residue and (b) banana pseudo-stem.

TG curves of the pyrolysis process was similar at different heating rates and could be roughly divided into three stages. Stage-I was the dehydration stage, with temperatures below 120 °C. The mass loss of pineapple residue and banana pseudo-stem during this stage was 4.92% and 7.14%, respectively. Stage-II was the main devolatilization stage, during which volatiles were mostly released and the mass loss accounted for about half. The main temperature range of this stage was 150–360 °C for pineapple residue and 160–370 °C for banana pseudo-stem. Peaks of DTG curves for pineapple residue and banana pseudo-stem appeared approximately at 300 °C and 280 °C, respectively. The maximum decomposition rates were 0.7532%/°C for pineapple residue and 0.4991%/°C for banana pseudo-stem. This difference could be associated to the content and structure of major components (hemicellulose, cellulose, lignin, and ash) [17]. The stronger decomposition peak of pineapple residue was due to higher content of hemicellulose and cellulose than that of banana pseudo-stem. Stage-III was the carbonization stage, which started at a temperature of above 370 °C. It was noticeable that a weak peak appeared at the temperature range of 600–700 °C in pyrolysis of banana pseudo-stem, which could be due to deep degradation of lignin [18]. The yield of final residue for pineapple residue and banana pseudo-stem was 22.50% and 32.69%, respectively. Compared with banana pseudo-stem, the final residue of pineapple residue was relatively lower, which was due to its higher volatile and lower ash in proximate analysis and ultimate analysis of Table 1.

DSC curves of pineapple residue and banana pseudo-stem at different heating rates are shown in Figure 2. The position of peaks in DSC curves was nearly consistent with that of DTG curves. An apparent endothermic peak occurred in the temperature range from the initial temperature to 150 °C due to evaporation of moisture. Compared to water evaporation, a weak endothermic process occurred in the temperature range of 250–400 °C, related to the decomposition of hemicellulose and cellulose. When the temperature was higher than 400 °C, the heat was continuously absorbed and associated to the decomposition of lignin and deep carbonization [19]. For banana pseudo-stem, a small endothermic peak occurred at around 650 °C, which might be attributed to high lignin content and its further degradation.

## 2.2. Pyrolysis Kinetics

### 2.2.1. Kinetics Based on the Friedman Method

In this section, pyrolysis kinetics was calculated based on the Friedman method (a multi-heating rate method) for both samples. In order to obtain kinetic parameters of main pyrolysis stages, the linear fitting plots were made by fitting  $\ln(\beta d\alpha/dT_\alpha)$  against  $1/T_\alpha$ . The lines fitted well and correlation coefficient was more than 0.99 at conversion rates ranging from 0.1 to 0.9. The activation energy could be obtained from the slope of the linear fitting plots, which are listed in Table 2. The activation energy of pineapple residue and banana pseudo-stem were about 159–335 kJ/mol and 169–364 kJ/mol, respectively. These data showed that decomposition of banana pseudo-stem generally required more energy than pineapple residue. It was attributed to the higher lignin content of banana pseudo-stem than that of pineapple residue, while the content of cellulose and hemicellulose was lower than that of pineapple residue. In addition, activation energy increased notably at conversion rates from 0.1 to 0.9, which could be due to cleavage reactions ranging from weak bonds to strong bonds [20].

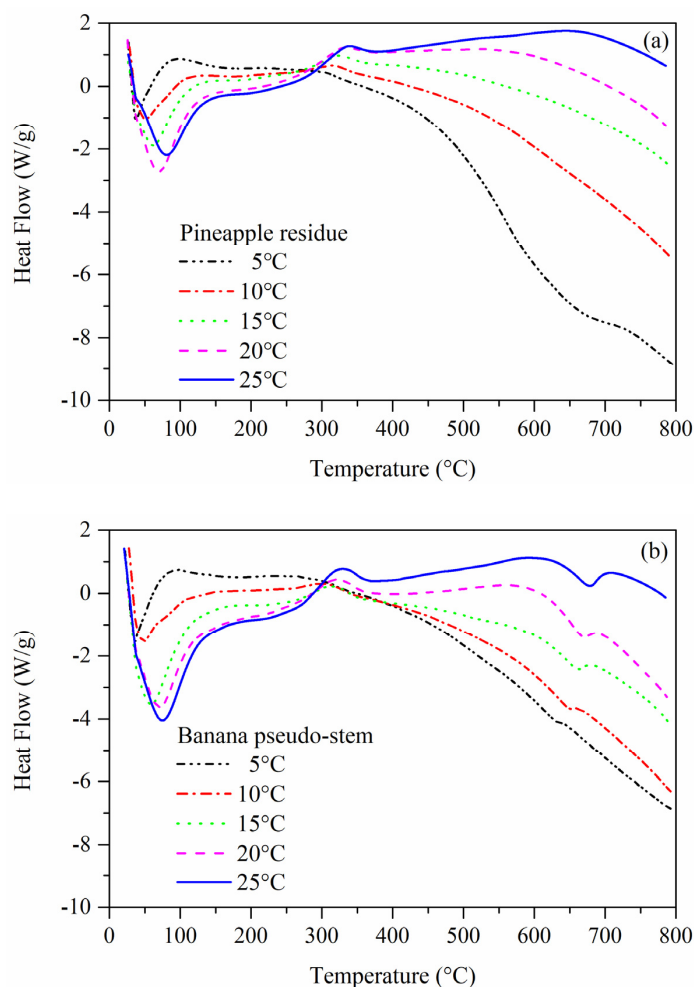


Figure 2. DSC curves of (a) pineapple residue and (b) banana pseudo-stem.

Table 2. Activation energy calculated by the Friedman method and pre-exponential factor at different conversion rates during pyrolysis.

Conversion Rates $\alpha$	Pineapple Residue			Banana Pseudo-Stem		
	Activation Energy $E_{\alpha}$ (kJ/mol)	Pre-Exponential Factor <sup>a</sup> $A$ (s <sup>-1</sup> )	Correlation Coefficient $R^2$	Activation Energy $E_{\alpha}$ (kJ/mol)	Pre-Exponential Factor $A$ (s <sup>-1</sup> )	Correlation Coefficient $R^2$
0.10	157	$1.98 \times 10^{15}$	0.992	178	$2.04 \times 10^{17}$	0.990
0.15	159	$2.50 \times 10^{15}$	0.991	169	$2.64 \times 10^{16}$	0.993
0.20	162	$4.88 \times 10^{15}$	0.991	170	$3.25 \times 10^{16}$	0.991
0.25	172	$4.49 \times 10^{16}$	0.993	174	$1.10 \times 10^{17}$	0.996
0.30	177	$1.56 \times 10^{17}$	0.992	176	$1.83 \times 10^{17}$	0.996
0.35	191	$3.45 \times 10^{18}$	1.000	181	$6.17 \times 10^{17}$	0.996
0.40	184	$8.09 \times 10^{17}$	0.996	185	$1.81 \times 10^{18}$	0.996
0.45	187	$1.54 \times 10^{18}$	0.997	192	$8.60 \times 10^{18}$	0.995
0.50	189	$3.19 \times 10^{18}$	0.995	201	$5.40 \times 10^{19}$	0.995
0.55	198	$2.22 \times 10^{19}$	0.996	217	$1.39 \times 10^{21}$	0.995
0.60	215	$6.08 \times 10^{20}$	0.995	240	$1.17 \times 10^{23}$	0.994
0.65	243	$1.60 \times 10^{23}$	0.995	276	$1.24 \times 10^{26}$	0.993
0.70	292	$1.37 \times 10^{27}$	0.995	321	$4.06 \times 10^{29}$	0.998
0.75	305	$1.43 \times 10^{27}$	0.993	334	$3.01 \times 10^{29}$	0.995
0.80	315	$1.75 \times 10^{29}$	0.990	345	$2.78 \times 10^{31}$	0.993
0.85	330	$1.66 \times 10^{29}$	0.990	350	$2.16 \times 10^{33}$	0.990
0.90	335	$2.03 \times 10^{31}$	0.991	364	$1.68 \times 10^{34}$	0.995

a: the pre-exponential factor was calculated after the determination of activation energy  $E_{\alpha}$  and mechanism function  $f(\alpha)$ .

In order to determine optimal mechanism function  $f(\alpha)$ , the temperatures  $T_\alpha$  corresponding to the peaks of DTG curves at five heating rates were firstly chosen, and the corresponding conversion rates  $\alpha$  and activated energy  $E_\alpha$  acquired previously were determined. The 40 kinetic mechanism functions (shown in Supplementary Materials) were used by fitting  $\ln f(\alpha)$  against  $\ln (\beta d\alpha/dT_\alpha) + E_\alpha/RT_\alpha$  in order to ensure the optimal one [21]. Among these different kinetic mechanism functions, the Avrami-Erofeev equation performed better as Equation (1) for both samples. The pre-exponential factors are obtained from the intercept of fitting lines and the corresponding value of the optimal  $f(\alpha)$ , which are also listed in Table 2. The pre-exponential factors of two samples were both higher than  $10^9 \text{ s}^{-1}$  and apparently increased from  $1.98 \times 10^{15}$  to  $1.68 \times 10^{34} \text{ s}^{-1}$ , which indicated high molecular collision rate and reactivity [22].

$$f(\alpha) = \frac{1}{3} (1 - \alpha) [-\ln(1 - \alpha)]^{-2} \quad (1)$$

### 2.2.2. Kinetics Based on the Deconvolution Method

Biomass pyrolysis was considered as an overlapped decomposition process of hemicellulose, cellulose, and lignin. The three components decomposed by parallel or competitive reactions, having unique physical and chemical properties [23]. The temperature ranges of hemicellulose, cellulose, and lignin degradation was generally at 210–345 °C, 260–390 °C, and 200–800 °C, respectively [24]. In this study, the deconvolution method (a multi-peak fitting method) was also applied in pyrolysis kinetics of biomass samples. DTG curves of pineapple residue and banana pseudo-stem were deconvoluted into several fitting peaks with Gaussian function. Figure 3 shows the deconvolution of DTG curves of pineapple residue and banana pseudo-stem at a heating rate of 5 °C/min. Other deconvolution curves, at different heating rates, are showed in the Supplementary Materials. DTG curves of pineapple residue were deconvoluted with three peaks, corresponding to hemicellulose, cellulose, and lignin. Kinetic parameters of deconvoluted DTG curves are given in Table 3. Activation energy of three deconvoluted peaks was 139.37, 186.99, and 276.00 kJ/mol. Considering the deep degradation of lignin and high ash content, DTG curves of banana pseudo-stem were deconvoluted with four peaks. Activation energy of four deconvoluted peaks was 174.18, 175.78, 280.37, and 364.80 kJ/mol. The optimal kinetic mechanism function for decomposition of both hemicellulose and cellulose was the Avrami-Erofeev equation, while optimal kinetic mechanism function for lignin decomposition was the J-M-A equation. Compared with Section 2.2.1, there was similar variation between the Friedman method and the deconvolution method. However, the difference value of kinetic parameters between the Friedman method and the deconvolution method was likely due to the interaction of components in biomass samples, which needs further research.

### 2.3. Evaluation of Thermodynamic Parameters

Figure 4 shows thermodynamic parameters during pyrolysis of pineapple residue and banana pseudo-stem at a heating rate of 5 °C/min. The enthalpy  $\Delta H$  during pyrolysis of pineapple residue and banana pseudo-stem was approximately 153–335 and 165–355 kJ/mol, respectively. It indicated that heat energy consumed by pineapple residue to dissociate bonds was generally less than that of banana pseudo-stem [25]. The difference between activation energy and  $\Delta H$  was around 4 kJ/mol. It was relatively easy to overcome potential energy barrier, which was necessary to form activated complexes [26]. When pyrolysis system is at the state of thermodynamic equilibrium, the difference of Gibbs free energy  $\Delta G$  is zero. The change of  $\Delta G$  during pyrolysis of pineapple residue and banana pseudo-stem was about 130–152 kJ/mol and 130–163 kJ/mol, respectively. It did not change much for each sample and reflected a potential of biomass used as bioenergy [27]. The entropy  $\Delta S$ , reflecting disorder degree in the system, was about 34–310 J/(mol·K) for pineapple residue and 68–360 J/(mol·K) for banana pseudo-stem. The positive  $\Delta S$  reflected an increase in the disorder of reaction. The high value of  $\Delta S$  indicated that the system had high reactivity and could generate activated complex faster [20,28].

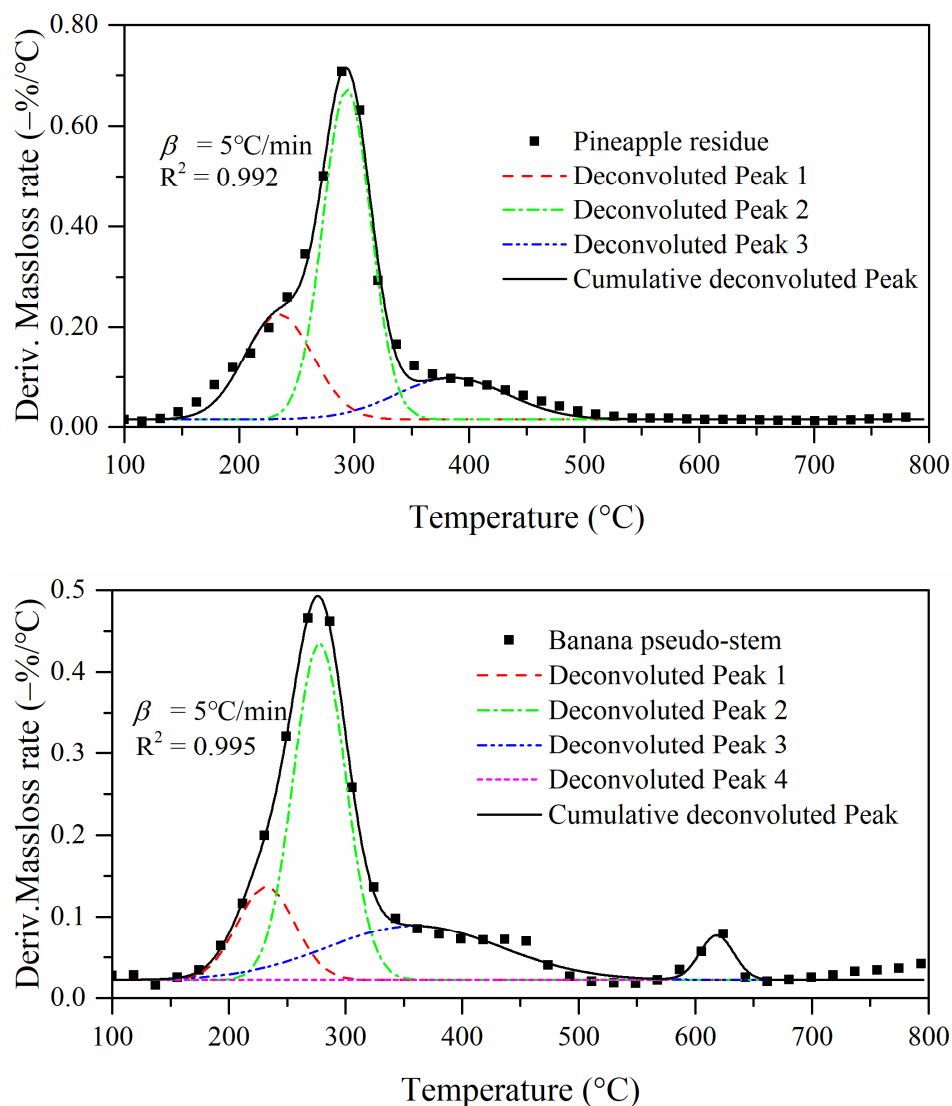
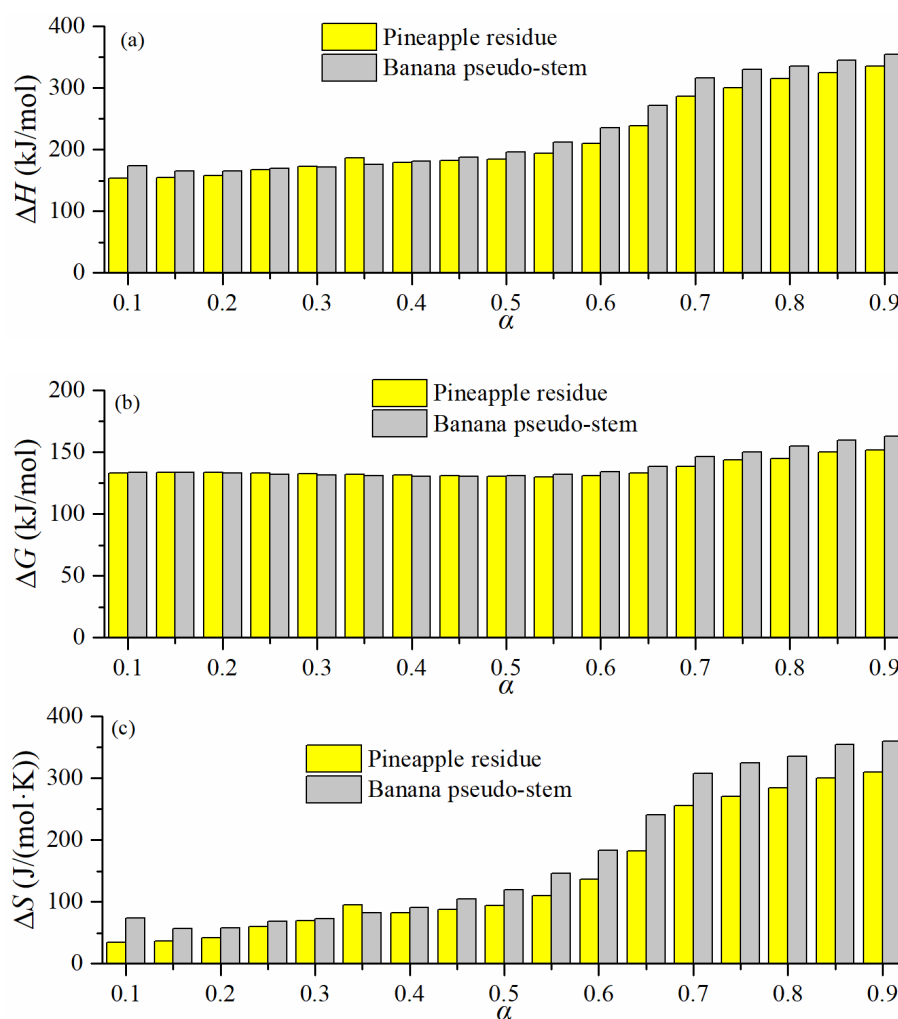


Figure 3. Deconvolution of DTG curves of pineapple residue and banana pseudo-stem with Gaussian function.

Table 3. Kinetic parameters of deconvoluted DTG curves.

Feedstock	Peak Temperature (°C)	Activation Energy <sup>a</sup>		Pre-exponential Factor A (s <sup>-1</sup> )	Mechanism Functions f(α)	Slope <sup>b</sup>	R <sup>2</sup>
		E <sub>α</sub> (kJ/mol)	R <sup>2</sup>				
Pineapple residue	233	139.37	0.994	2.0 × 10 <sup>14</sup>	$\frac{1}{4}(1 - \alpha)[- \ln(1 - \alpha)]^{-3}$	1.04	0.91
	294	186.99	0.997	1.3 × 10 <sup>18</sup>	$\frac{1}{2}(1 - \alpha)[- \ln(1 - \alpha)]^{-1}$	1.09	0.96
	385	276.00	0.998	3.6 × 10 <sup>21</sup>	$0.17(1 - \alpha)[- \ln(1 - \alpha)]^{1 - \frac{1}{0.17}}$	1.02	0.98
Banana pseudo-stem	232	174.18	0.989	1.6 × 10 <sup>17</sup>	$\frac{1}{4}(1 - \alpha)[- \ln(1 - \alpha)]^{-3}$	1.03	0.95
	278	175.78	0.993	1.5 × 10 <sup>17</sup>	$\frac{1}{2}(1 - \alpha)[- \ln(1 - \alpha)]^{-1}$	1.04	0.93
	359	280.37	0.965	1.2 × 10 <sup>22</sup>	$0.12(1 - \alpha)[- \ln(1 - \alpha)]^{1 - \frac{1}{0.12}}$	0.98	0.90
	618	364.80	0.980	2.2 × 10 <sup>22</sup>	$0.26(1 - \alpha)[- \ln(1 - \alpha)]^{1 - \frac{1}{0.26}}$	0.98	0.95

a: it was calculated via the Friedman method at the maximum mass loss zone for deconvoluted DTG curves;  
 b: the slope indicated the optimal mechanism functions when it reached to one during linear fitting operation.



**Figure 4.** Thermodynamic parameters at a heating rate of 5 °C/min. (a) enthalpy, (b) Gibbs free energy, and (c) entropy.

Thermodynamic parameters of the deconvoluted peaks in Section 2.2.2 for two samples were also calculated. The difference between activation energy and  $\Delta H$  of three deconvoluted peaks was 4.19, 4.72 and 5.56 kJ/mol for pyrolysis of pineapple residue, and 4.22, 4.56 and 5.43 kJ/mol for pyrolysis of banana pseudo-stem. It reflected higher difficulty for the formation of activated intermediates from lignin than that of cellulose and hemicellulose. The  $\Delta G$  during pyrolysis of three deconvoluted peaks was 127.01, 132.35, and 170.01 kJ/mol for pyrolysis of pineapple residue, which was 133.74, 132.44, and 172.12 kJ/mol for banana pseudo-stem. It was likely due to the difference in chemical composition and structures between two samples. At the same time, the  $\Delta S$  of three deconvoluted peaks was 16.12, 88.08 and 152.64 kJ/(mol·K) for pineapple residue, which was 71.74, 70.27, and 162.76 kJ/(mol·K) for banana pseudo-stem. The  $\Delta S$  and  $\Delta G$  for lignin was significantly higher, which revealed that lignin pyrolysis had the highest degree of disorder.

#### 2.4. Characterization of Volatiles during Pyrolysis

The three-dimensional FTIR distribution of evolved volatiles during pyrolysis of pineapple residue and banana pseudo-stem, at a heating rate of 25 °C/min, are both shown in Supplementary Materials. There were apparent absorbance peaks at 330 °C and 310 °C for banana pseudo-stem and pineapple residue, respectively. The intensity of volatiles produced from pineapple residue pyrolysis was significantly higher than that of banana pseudo-stem. There were apparent absorption peaks at 1176, 1774, 2354, 2962, and



3568  $\text{cm}^{-1}$  corresponding to O-containing functional groups, C=O stretching vibrations, C=O asymmetric stretching vibrations, C–H stretching vibrations, and O–H stretching vibrations. The main evolved compounds were  $\text{H}_2\text{O}$ ,  $\text{CH}_4$ ,  $\text{CO}_2$ ,  $\text{CO}$ , and various organic volatiles (acids, ketones, aldehydes, alcohols, phenols, and ethers).

The composition of evolved volatiles corresponding to the highest intensity of thermal decomposition was also analyzed by GC-MS. The name and content of compounds in volatiles are shown in Supplementary materials. Figure 5 shows the carbon number distribution of volatiles. The main carbon number was  $\text{C}_4$  and  $\text{C}_5$  for pineapple residue, and that was  $\text{C}_2$  and  $\text{C}_3$  for banana pseudo-stem. The results indicated different composition between crude bio-oils after condensation for both biomass samples. The carbon number of volatiles was both less than ten for pineapple residue and banana pseudo-stem, which indicated that volatiles could be upgraded into biomass-based gasoline.

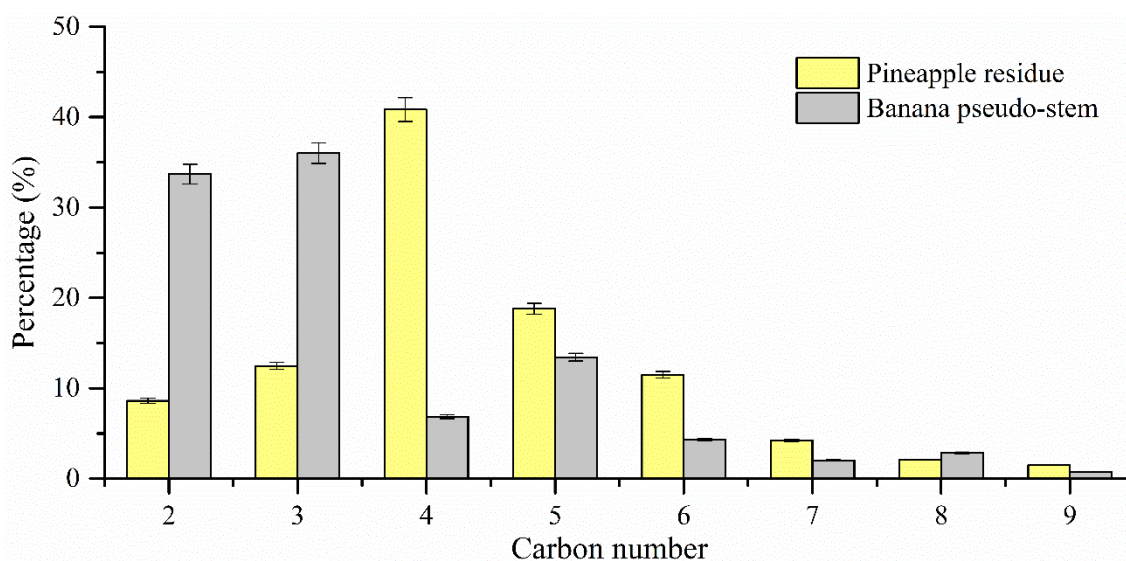


**Figure 5.** Carbon number distribution of volatiles sourced from pyrolysis at a heating rate of 25 °C/min.

Figure 6 shows distribution of compound type in volatiles during pyrolysis of two samples. The main types of compounds were acids, alcohols, aldehydes, esters, phenols, ketones, and furans. Acids were common compounds in pyrolysis oil. The main acid produced by pyrolysis of pineapple residue was acetoxyacetic acid, which accounted for ~30.41% of GC-MS peak areas. The main acid produced by pyrolysis of banana stems was acetic acid, which accounted for ~33.71% of GC-MS peak areas. Phenols mainly came from cleavage of lignin [29], which accounted for 4.70% of pineapple residue and 4.33% for banana pseudo-stem. Furfural and 2,3-Dihydro-1-benzofuran were two classic furans from biomass pyrolysis [24]. Both substances were present in the pyrolysis of pineapple residue and banana pseudo-stem. The furfural was produced due to dehydration, cyclization and demethoxy or methanol removal reaction. 2,3-Dihydro-1-benzofuran was derived from free radical reaction, cyclization reaction and hydrogenation reaction. Carbonyl compounds, such as ketones and aldehydes, generally originated from cleavage and condensation reaction. The content of aldehydes was relatively low, accounting for 3.02% and 1.20% for pineapple residue and banana pseudo-stem, respectively. There was a large quantity of ketones (mainly hydroxyacetone) in the evolved gas for banana pseudo-stem, which accounted for 43.94% of GC-MS peak areas. Alcohols were generally produced by demethylation reaction of methoxyl groups. Cyclopropyl carbinol was the main alcohol compound and its content was 3.97% and 3.90% in bio-oil produced by pineapple residue and banana pseudo-stems. Esters were also abundantly presented in the volatiles of pineapple residue. It was likely due to esterification reaction between alcohol, phenols and acids.

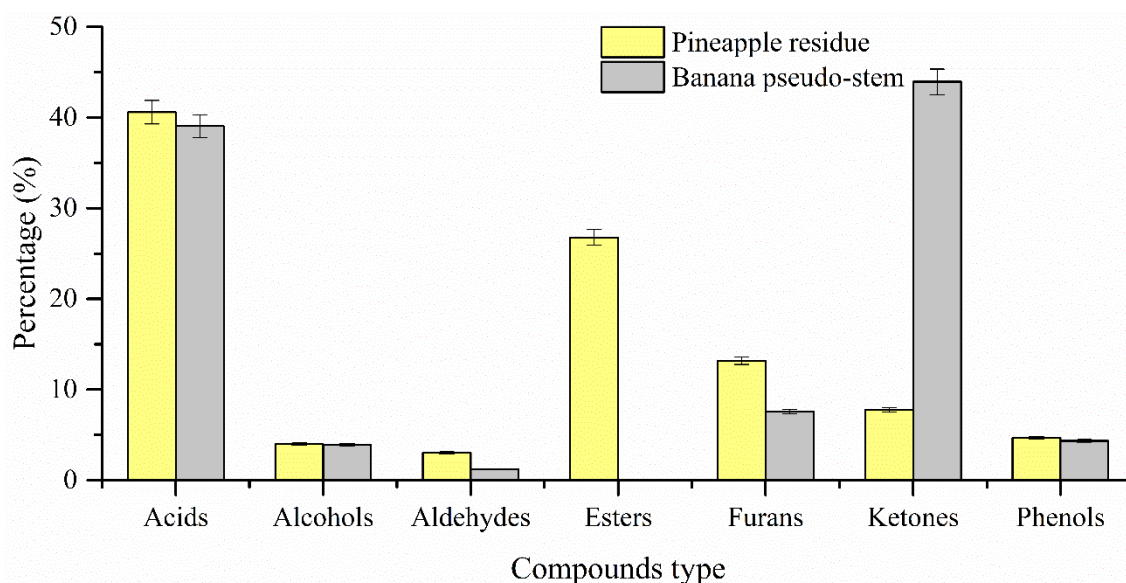


**Figure 6.** Compound types of volatiles and their distribution during pyrolysis at a heating rate of 25 °C/min.

### 2.5. Pyrolysis Mechanism

In this section, the relationship between key components (cellulose, hemicellulose, and lignin) in biomass and deconvoluted peaks in kinetics is shown in Figure 7, based on the results of TG/DTG, DSC, kinetics, thermodynamics, and composition of volatiles. Hemicellulose had the lowest pyrolysis temperature zone in the deconvoluted DTG curves as it consisted of short chains of saccharides, such as xylose, mannose, glucose, and galactose. At about 230 °C, activation energy of deconvoluted hemicellulose peak for pineapple residue and banana pseudo-stem was 139 kJ/mol and 174 kJ/mol, respectively. For comparison, the pyrolysis conversion rate of pineapple residue and banana pseudo-stem was about 10%, and the corresponding activation energy of raw biomass was 157 kJ/mol and 178 kJ/mol, respectively. Additionally, the degradation of short-chain saccharides during pyrolysis released a large amount of CO, CO<sub>2</sub>, and acids.

Cellulose is composed of the long-chain polymer with a high crystalline degree of glucose. The high crystallinity can enhance thermal stability of cellulose [30]. When the conversion rate of pineapple residue and banana pseudo-stem during pyrolysis reached, at about 35%, activation energy of pineapple residue and banana pseudo-stem increased to 191 kJ/mol and 181 kJ/mol, respectively. At this stage, the decomposition process of deconvoluted cellulose reached its peak, and began to decompose in a large amount. The activation energy of deconvoluted cellulose for pineapple residue and banana pseudo-stem was 187 kJ/mol and 176 kJ/mol, respectively. In addition to CO, CO<sub>2</sub>, and acids, the volatiles during pyrolysis of cellulose contained furans such as furfural and 2,3-dihydro-1-benzofuran.

Lignin is thermally stable compared with cellulose and hemicellulose. It contains aromatic rings with various oxygen-containing functional groups, and these aromatic rings are connected with different bonding modes. It led to a complexity of decomposition and a wider pyrolysis temperature range [17]. The activation energy of deconvoluted lignin for pineapple residue and banana pseudo-stem was 276 kJ/mol and 280 kJ/mol, respectively. When the conversion rate of samples reached about 70%, a large amount of lignin decomposed, and the activation energy of raw biomass (pineapple residue and banana stems) increased significantly to 292 kJ/mol and 321 kJ/mol. The decomposition of lignin caused the formation of phenols, such as phenol, guaiacol and 2-methoxy-4-vinylphenol. Banana stems had a high lignin content, which apparently affected pyrolysis

characterization of biomass and interactions between key biomass components, and also intensified complexity of kinetics and pyrolysis mechanism.

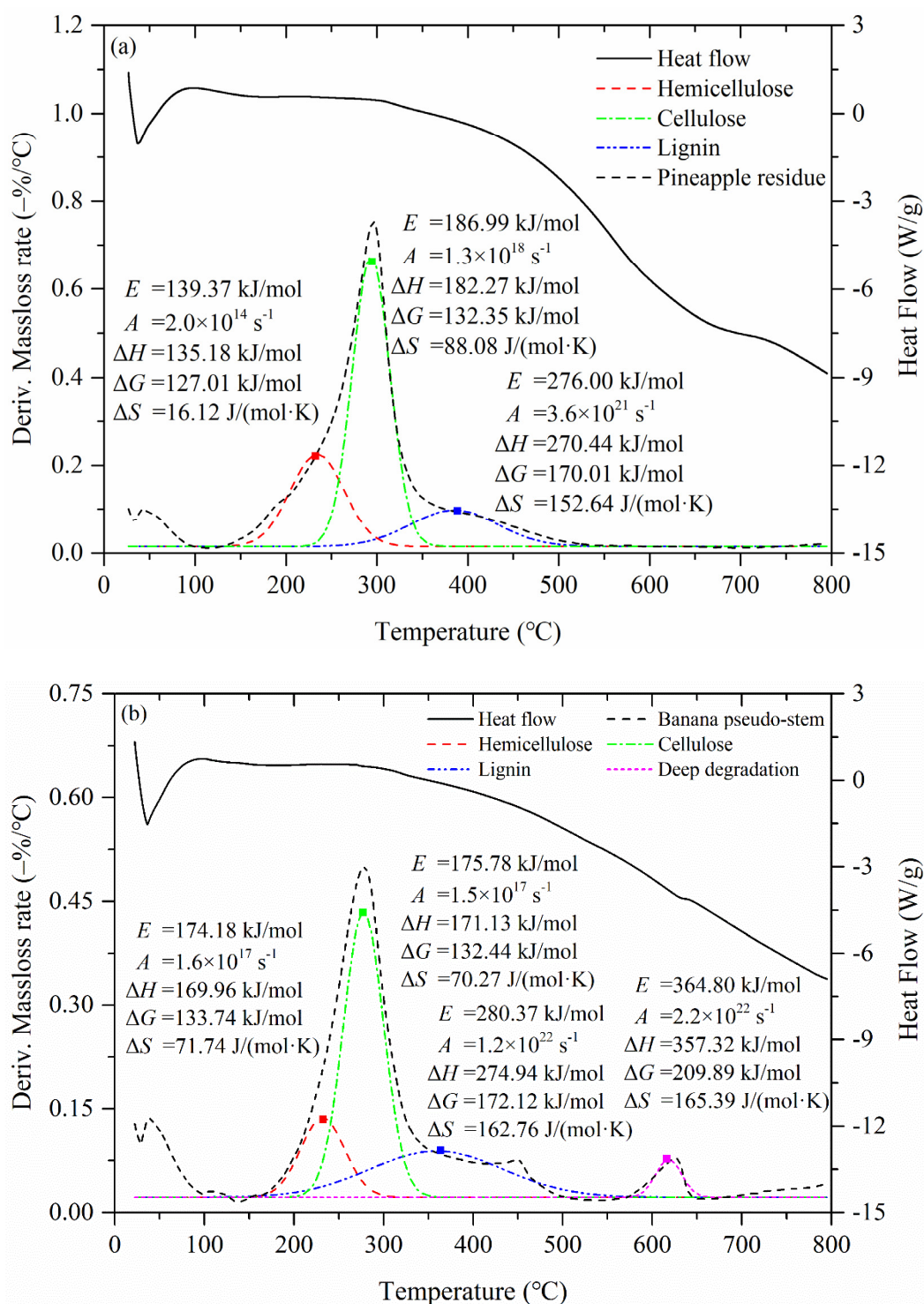


**Figure 7.** Relationship between key components in biomass and deconvoluted peaks in kinetics (a) pineapple residue and (b) banana pseudo-stem.

## 2.6. Electrochemical Performance of Biomass-Derived Porous Carbon

Bio-char is one of the main products of biomass pyrolysis, which can be activated with KOH into porous carbon. At 500 °C, the yield of bio-char for pineapple residue and banana pseudo-stems was  $35.3 \pm 0.4\%$  and  $42.8 \pm 0.4\%$ , respectively. After activation

with KOH in different ratios of 1:1, 1:3, and 1:5 at 700 °C, the yield of porous carbon was  $37.4 \pm 0.5\%$ ,  $33.5 \pm 0.7\%$ , and  $27.7 \pm 0.6\%$  based on bio-char, respectively. In this section, electrochemical performance of porous carbons was evaluated to reveal the potential of biomass feedstocks as electrochemical materials.

The specific surface area, micropore area, and pore volume for bio-chars and porous carbons, calculated by the t-plot method, are listed in Table 4. N<sub>2</sub> adsorption-desorption isotherms and pore distribution of bio-chars and porous carbons are shown in Supplementary Materials. The porous carbon dominated by micropores was effectively formed through KOH activation. The pores of PR-1, PR-3, and BP-1 mainly distributed in 0.5–1.0 nm. This micropore structure was beneficial to improve the capability of charge storage. While the pores of PR-5 and BP-3 distributed in a certain number of narrow micropores (0.5–1.0 nm), they also have wider micropores (1–2 nm). Wider micropores (1–2 nm) in porous carbon could facilitate transportation of electrolyte ions [12]. As for BP-5, its surface area was significantly reduced because of over activation of KOH and the collapse of pores, which was indicated by SEM images (presented in Supplementary materials).

**Table 4.** Surface area and pore characteristics of bio-chars and porous carbons.

Samples	Surface Area (m <sup>2</sup> /g)	Micropore Area (m <sup>2</sup> /g)	Pore Volume (cm <sup>3</sup> /g)	Correlation Coefficient
PR <sup>a</sup>	329.3	249.6	0.200	0.991
PR-1	1072.2	914.4	0.489	0.997
PR-3	1634.1	1287.4	0.831	0.995
PR-5	2377.7	1192.5	1.267	0.996
BP <sup>b</sup>	308.1	178.3	0.204	0.995
BP-1	1260.4	1000.5	0.683	0.997
BP-3	2312.6	1390.9	1.147	0.998
BP-5	1276.4	328.1	0.933	0.997

a: PR means bio-char sourced from pineapple residue; b: BP means bio-char sourced from banana pseudo-stem.

Porous carbon are promising materials for energy storage due to their high surface area, high conductivity, and outstanding cyclic capability. The porous carbons were further prepared into electrode materials in this study and their electrochemical performance (BP-1, BP-3, BP-5, PR-1, PR-3, and PR-5) was assessed by cyclic voltammetry (CV) and galvanostatic charge/discharge (GCD). Figure 8 displays CV curves of electrode materials at a scanning rate of 5 mV/s in the range of 0.1 to 0.0 V. The CV curves basically maintained a rectangular shape and indicated typical properties of electrical double-layer capacitance. The area relationship of the CV curve of electrode materials sourced from pineapple residue was PR-5 > PR-3 > PR-1, and it was BP-3 > BP-1 > BP-5 for electrode materials sourced from banana pseudo-stems, reflecting their corresponding capability of charge storage.

The capacitive performance of porous carbon derived electrode materials was further investigated with galvanostatic charge/discharge. Figure 9 shows GCD curves of electrode materials at current density of 0.5 A/g. The relationship of charge/discharge time of all electrode materials was consistent with their relationship of the CV curves. The electrode materials (PR-5 and BP-3) with relatively high capacitance values were further compared by cyclic stability analysis. The GCD curves of PR-5 and BP-3 under different current densities were displayed in Supplementary Materials, which remained the shape of isosceles triangle, reflecting favorable properties of ion diffusion and electron exchange [11]. Specific capacitance of PR-5 and BP-3 calculated by Equation (9) based on the GCD curves are listed in Table 5. As the current density increased from 0.5 A/g to 8 A/g, capacitance retention of PR-5 and BP-3 were 71.78% and 71.72%, respectively. The results demonstrated excellent rate performance for PR-5 and BP-3. In conclusion, pineapple residue and banana pseudo-stem were potential raw materials for production of porous carbons.

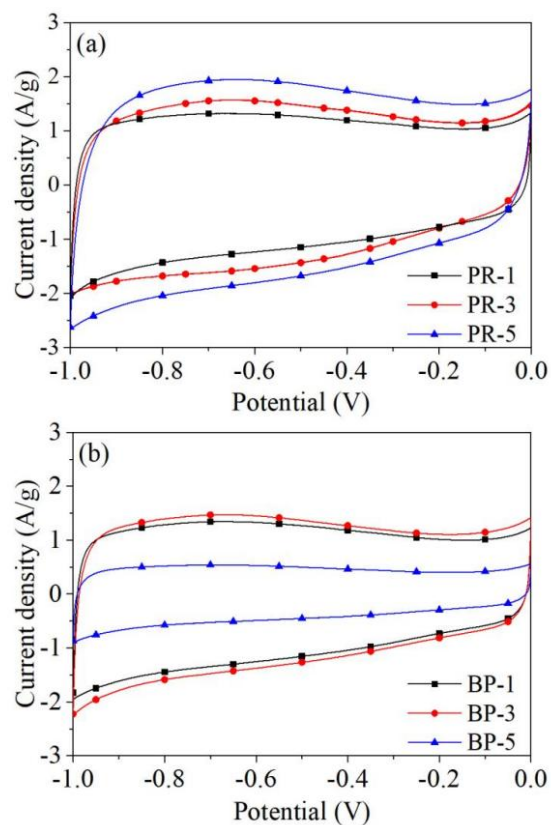


**Figure 8.** Cyclic voltammetry (CV) curves of porous carbons sourced from (a) pineapple residue and (b) banana pseudo-stem at the scan rate of 5 mV/s.

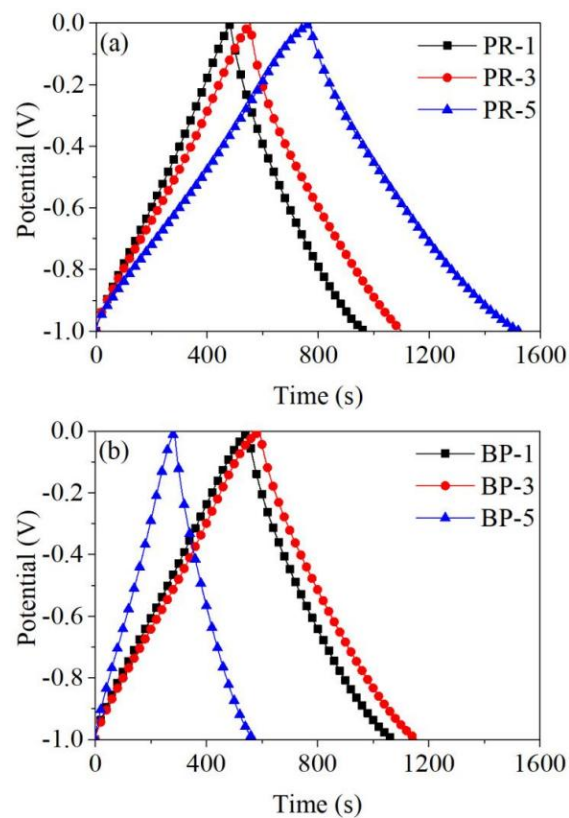


**Figure 9.** Galvanostatic charge/discharge (GCD) curves of porous carbons sourced from (a) pineapple residue and (b) banana pseudo-stem at current density of 0.5 A/g.

**Table 5.** Specific capacitance of PR-5 and BP-3 at different current densities.

Samples	Specific Capacitance (F/g)					
	0.5A/g	1A/g	2A/g	4A/g	6A/g	8A/g
PR-5	374.5 ± 4.1	358.1 ± 0.4	321.8 ± 3.5	298.8 ± 3.3	283.2 ± 3.1	268.8 ± 3.0
BP-3	296.7 ± 3.3	280.3 ± 3.1	247.0 ± 2.7	229.6 ± 2.5	220.2 ± 2.4	212.8 ± 2.3

### 3. Materials and Methods

#### 3.1. Materials

Biomass waste (pineapple residue and banana pseudo-stem) was collected from Guangdong Province, China. Banana pseudo-stem was the stalk of the plant, while pineapple residue was the crown and peel of the plant. Both samples were dried for 24 h at 105 °C to remove water. The dried samples were then ground by a micro plant grinder and sieved into fine powder, with a diameter of 0.38–0.25 mm. Proximate analysis (Kaiyuan 5E-MAG6700, Changsha, China) was conducted following Chinese standard (GB/T 212–2001), which was equivalent to ISO 562, 1171, and 11722. Ultimate analysis (Elementar Vario EL, Langensfeld, Germany) of biomass was also conducted and shown in Table 1. The content of elemental oxygen was calculated based on 100% reduction by the content of elemental C, H, N, S, and ash in samples. The heating value of the samples was measured by a bomb calorimeter (PARR 1281, St. Albans, WV, USA) and the calorimeter was calibrated with benzoic acid (26470 ± 20 J/g) before each measurement.

Additionally, the Van Soest method was adopted to effectively segregate and determine the content of hemicellulose, cellulose, and lignin. Samples were firstly boiled with a neutral detergent and the insoluble residue was named as neutral detergent fiber, which mainly included hemicellulose, cellulose, lignin, and silicate. This neutral detergent fiber was further treated with an acid detergent, and the remaining residue was named as acid detergent fiber including cellulose, lignin, and silicate. The mass difference between neutral detergent fiber and acid detergent fiber was the content of hemicellulose in biomass. The acid detergent fiber was treated with 72% H<sub>2</sub>SO<sub>4</sub> solution, and the remaining residue (named as RM) was lignin and silicate. The mass difference between the acid detergent fiber and the remaining residue RM was the content of cellulose in samples. The remaining residue RM was incinerated at 550 °C, and the mass which escaped during incineration was the content of lignin [31].

#### 3.2. Thermogravimetric Experiments

Thermogravimetric experiments were carried out from ambient temperature to 800 °C under five heating rates (5, 10, 15, 20, and 25 °C/min) using a thermal analyzer (Thermal Analysis SDTQ600, New Castle, DE, USA). The samples were dried prior to each experiment at 105 °C. The balance gas and sample gas were both nitrogen gas (99.999%) and their flow rates were set as 100.0 mL/min in order to provide an inert environment and prevent oxidation. The sample (~6 mg) was put in an alumina pan for each run.

#### 3.3. Kinetic Models and Calculation

Pyrolysis of samples can be generally simplified into a reaction: Biomass (solid) → Bio-char + Volatiles. Equation (2) can be expressed as its reaction rate, where  $\alpha$  is the conversion rate (%),  $t$  is the reaction time (s),  $k$  is the rate constant (s<sup>-1</sup>), and  $f(\alpha)$  represents a mechanism function related to reactants and reaction rate. The form of  $f(\alpha)$  depends on reaction mechanism during pyrolysis.

$$d\alpha/dt = k f(\alpha) \quad (2)$$

Substituting the Arrhenius equation into Equation (2), Equation (3) is obtained.  $A$  is the pre-exponential factor (s<sup>-1</sup>),  $E_{\alpha}$  is the activation energy (kJ/mol),  $R$  is the gas constant

( $R = 8.314 \times 10^{-3}$  kJ/(mol·K)), and  $T_\alpha$  is pyrolysis temperature ranged from ambient temperature to 800 °C in this study.

$$d\alpha/dt = Ae^{-E_\alpha/RT_\alpha} f(\alpha) \quad (3)$$

At a constant heating rate ( $\beta = dT/dt$ ), the kinetic equation can be transformed into Equation (4).

$$d\alpha/dT_\alpha = A/\beta e^{-E_\alpha/RT_\alpha} f(\alpha) \quad (4)$$

Taking the napierian logarithm of Equation (4) with some modifications, Equation (5) is obtained. Pyrolysis kinetics was calculated based on this equation and the introduction of the Friedman method and the deconvolution method is as follow.

$$\ln(\beta d\alpha/dT_\alpha) = \ln A + \ln[f(\alpha)] - E_\alpha/RT_\alpha \quad (5)$$

### 3.3.1. Friedman Method

Kinetic analysis was firstly determined by the Friedman method (a multi-heating rate method in the range of 5–25 °C/min) based on Equation (5). This method does not need to assume mechanism functions during the calculation of activation energy, avoiding error caused thereby. By plotting  $\ln(\beta d\alpha/dT_\alpha)$  against  $1/T_\alpha$  at selected conversions,  $E_\alpha$  can be obtained from the slope of fitting plots. Conversion rates ranging from 0.10 to 0.90 with a step of 0.05 were selected to determine activation energy in this multi-heating rate method.

Then, the determination of the optimal mechanism function  $f(\alpha)$ , the temperatures  $T_\alpha$  corresponding to the peaks of DTG curves at five heating rates were firstly chosen, and the corresponding conversion rates  $\alpha$  and activated energy  $E_\alpha$  acquired before were determined. By plotting  $\ln f(\alpha)$  against  $\ln(\beta d\alpha/dT_\alpha) + E_\alpha/RT_\alpha$  with all kinds of  $f(\alpha)$ , the optimal mechanism function can be selected, which makes the slope of fitting plots to nearly reach one. Finally, the pre-exponential factor  $A$  can be determined, according to the obtained  $E_\alpha, f(\alpha)$  and intercept of fitting lines [21]. This is a key step to determine kinetics parameters for understanding pyrolysis reaction.

### 3.3.2. Deconvolution Method

Biomass pyrolysis process includes many chemical reactions, which can be divided into several hypothetical reactions by mathematical methods. The deconvolution method (Gaussian multi-peak fitting method) via Origin software (Version 9.1) was used to deconvolute DTG curves with several fitting peaks (Equation (6)). It gave us fitting results based on accuracy automatically. A fitting peak number was defined as three or four based on biomass components and fitting accuracy mathematically. Then, the kinetic parameters of each fitting peak were further determined with the same method in Section 3.3.1 in order to discuss pyrolysis mechanism. The detailed procedure can also refer to our previous research [21].

$$\sum_{i=1}^n \ln(\beta d\alpha/dT_\alpha) = \sum_{i=1}^n (\ln A + \ln[f(\alpha)] - E_\alpha/RT_\alpha) \quad (6)$$

where  $n$  is the number of fitting peaks in deconvolution process ( $n$  is three for pineapple residue and it is four for banana pseudo-stem in this study).

### 3.4. Thermodynamic Parameters Calculation

Thermodynamic parameters can reflect the potential of biomass waste as bioenergy, which include enthalpy ( $\Delta H$ , kJ/mol), Gibbs free energy ( $\Delta G$ , kJ/mol), and entropy ( $\Delta S$ , kJ/(mol·K)). The values of these parameters were based on the kinetic parameters in Section 3.3 and calculated with Equation (7)–(9), respectively [25,27,32].

$$\Delta H = E_\alpha - RT_\alpha \quad (7)$$

$$\Delta G = E_\alpha + RT_m \ln(K_B T_m/hA) \quad (8)$$

$$\Delta S = (\Delta H - \Delta G)/T_m \quad (9)$$

where  $T_\alpha$  is the temperature corresponding to conversion  $\alpha$ ,  $T_m$  is the temperature at the peak of the DTG curve,  $K_B$  is the Boltzmann constant ( $K_B = 1.381 \times 10^{-26}$  kJ/ K) and  $h$  is the Plank constant ( $h = 6.626 \times 10^{-34}$  J · s).

### 3.5. Online analysis of Volatiles during Pyrolysis

Evolved volatiles during biomass pyrolysis were analyzed via a hyphenated equipment of TG-FTIR-GCMS. The evolved volatiles enter the FTIR and GCMS through a transmission line (PerKinElmer TL9000, Waltham, MA, USA), which is kept at 280 °C. Hyphenated techniques can simplify collection of pyrolysis products and effectively avoid mass loss caused by condensation. TG experiment was conducted from ambient temperature to 800 °C at a heating rate of 25 °C/min using a thermal analyzer (PerKinElmer TGA 8000, Waltham, MA, USA). Fourier transform infrared spectroscopy analysis (PerKinElmer Frontier FTIR, Waltham, MA, USA) was performed at the wavenumber of 4000–650  $\text{cm}^{-1}$  with an interval range of 1  $\text{cm}^{-1}$ . Gas chromatography-mass spectrometry analysis (PerKinElmer Clarus SQ8T, Waltham, MA, USA) with an Elite-5MS chromatographic column (30 m and 0.25 mm ID) was performed to analyze the composition of evolved volatiles at the maximum mass loss zone of TG curves. The scan range of mass spectrometer was from 50 to 300 mass units. Compounds in evolved volatiles were identified using the mass spectral library (NIST 14) by operation software TurboMas (Version 6.1.0, Waltham, MA, USA). The percentage of each compound in pyrolysis products was determined by the percentage of chromatographic peak area.

### 3.6. Electrochemical Analysis of Porous Carbons

Biomass was firstly carbonized to obtain bio-chars at 500 °C for 1.5 h in a fixed bed reactor under a nitrogen environment (Zhonghuan SX3-4-13, China). Pyrolysis product bio-chars were further activated into porous carbons chemically, and evaluated in an electrochemical experiment system to reveal their potential as electrode materials. The obtained bio-char and KOH (AR) were mixed with mass ratios of 1:1, 1:3, and 1:5, and chemically activated at 700 °C under nitrogen environment for an hour in the fixed bed reactor [33]. Then, this mixture after activation was washed with 10% HCl solution and deionized water consecutively, until the washing solution was neutral. The obtained porous carbons were dried at 100 °C for 12 h and designated as PR- $n$  and BP- $n$  ( $n = 1, 3, 5$ ), respectively. PR referred to pineapple residue and BP referred to banana pseudo-stem. For comparison, raw biomass was also carbonized at 700 °C for 2.5 h without activation and designated as PR and BP, respectively. The specific surface areas and pore distribution were evaluated for all bio-chars and porous carbons through the Surface areas and Porosity Analyzer (Micromeritics, ASAP 2020 HD88, Norcross, GA, USA) at  $-196.15$  °C. Samples were degassed at 200 °C for 12 h before measurement. Isotherm data was taken over the partial pressure range of 0.0–1.0 using nitrogen gas (99.999%).

To evaluate electrochemical performance of porous carbons, they were mixed with acetylene black and polytetrafluoroethylene with the ratio of 75: 20: 10 by weight. The mixtures were made into uniform sheets and dried at 80 °C for 12 h. The sheets were pressed on a nickel foam current collector (1 cm × 1 cm) (purchased from Tianjin Aiweixin Chemical Technology, Tianjin, China) at 10 MP to obtain electrode materials. The electrochemical performance of obtained electrode materials was analyzed in a three-electrode system by an electrochemical workstation (CHI 660E, Shanghai, China). The electrodes prepared from porous carbons were the working electrode, the platinum was the auxiliary electrode, the calomel was the reference electrode, and 6 mol/L KOH solution was the electrolyte solution. Cyclic voltammetry (CV) and galvanostatic charge/discharge (GCD) were assessed by



the three-electrode experiment system. Specific capacitance of electrode materials was determined based on the Equation (10) with GCD data.

$$C = \frac{I\Delta t}{\Delta V m} \quad (10)$$

where  $I$  refers to the discharging current,  $\Delta t$  is the discharging time, the potential range of  $\Delta V$  is the voltage drop upon discharge excluding the IR drop,  $m$  is mass of the active materials.

#### 4. Conclusions

Pyrolysis of banana pseudo-stem and pineapple residue was conducted by TG, FTIR, and GC-MS. DTG curves were divided into three or four fitting peaks based on key composition (cellulose, hemicellulose, and lignin) with the deconvolution method and Gaussian function. The resulted kinetics after deconvolution were more suitable for biomass pyrolysis. As pyrolysis reaction proceeded, cellulose, hemicellulose, and lignin gradually decomposed, and the energy required, and reactivity of pyrolysis process, gradually increased. The volatiles produced from pineapple residue pyrolysis were significantly higher than that of banana pseudo-stem. The main evolved compounds were H<sub>2</sub>O, CH<sub>4</sub>, CO<sub>2</sub>, CO, and various organic volatiles (acids, ketones, aldehydes, alcohols, phenols, and ethers). Porous carbons derived from pineapple residue and banana pseudo-stem exhibited high specific area (>1000 m<sup>2</sup>/g) and good capacitance performance (374.5 F/g and 296.7 F/g at 0.5 A/g), which provided an important pathway for valorization of pineapple residue and banana pseudo-stem.

**Supplementary Materials:** The following supporting information can be downloaded at: <https://www.mdpi.com/article/10.3390/catal12080840/s1>, Figure S1 Peak deconvolution of DTG curves of pineapple residue at a heating rate of 10 °C/min; Figure S2 Peak deconvolution of DTG curves of pineapple residue at a heating rate of 15 °C/min; Figure S3 Peak deconvolution of DTG curves of pineapple residue at a heating rate of 20 °C/min; Figure S4 Peak deconvolution of DTG curves of pineapple residue at a heating rate of 25 °C/min; Figure S5 Peak deconvolution of DTG curves of banana pseudo-stem at a heating rate of 10 °C/min; Figure S6 Peak deconvolution of DTG curves of banana pseudo-stem at a heating rate of 15 °C/min; Figure S7 Peak deconvolution of DTG curves of banana pseudo-stem at a heating rate of 20 °C/min; Figure S8 Peak deconvolution of DTG curves of banana pseudo-stem at a heating rate of 25 °C/min; Figure S9 Three-dimensional FTIR distribution of evolved gas during pyrolysis ((a) pineapple residue and (b) banana pseudo-stem); Figure S10 (a) N<sub>2</sub> adsorption-desorption isotherms and (b) pore distribution of bio-chars and porous carbons sourced from pineapple residue; Figure S11 (a) N<sub>2</sub> adsorption-desorption isotherms and (b) pore distribution of bio-chars and porous carbons sourced from banana pseudo-stems; Figure S12 Galvanostatic charge/discharge (GCD) curves of (a) PR-5 and (b) BP-3 at different current densities; Figure S13 SEM images of porous carbon sourced from pineapple residue and banana pseudo-stem (a) BP-1, (b) BP-3, (c) BP-5, (d) PR-1, (e) PR-3, and (f) PR-5; Table S1 Pyrolysis mechanism function; Table S2 Pyrolysis thermodynamic parameters of the deconvoluted peaks; Table S3 The relative content of main volatile organic compounds sourced from pineapple residue; Table S4 The relative content of main volatile organic compounds sourced from banana pseudo-stem.

**Author Contributions:** Funding acquisition, B.S.; Investigation, S.Y.; Software, J.Y.; Supervision, X.W.; Writing—original draft, X.W.; Writing—review & editing, L.X. All authors have read and agreed to the published version of the manuscript.

**Funding:** The project was supported by the Joint Funds of the National Natural Science Foundation of China (U20A20302), Natural Science Foundation of Hebei, China [E2020202006] and Natural Science Foundation of Tianjin, China [20JCYBJC00740].

**Conflicts of Interest:** The authors declare no conflict of interest.

## References

1. Dhyani, V.; Bhaskar, T. A comprehensive review on the pyrolysis of lignocellulosic biomass. *Renew. Energy* **2018**, *129*, 695–716. [[CrossRef](#)]
2. Sánchez, J.D.; Ramírez, G.E.; Barajas, M.J. Comparative kinetic study of the pyrolysis of mandarin and pineapple peel. *J. Anal. Appl. Pyrol.* **2016**, *118*, 192–201. [[CrossRef](#)]
3. Taib, R.M.; Abdullah, N.; Aziz, N.S.M. Bio-oil derived from banana pseudo-stem via fast pyrolysis process. *Biomass Bioenergy* **2021**, *148*, 106034. [[CrossRef](#)]
4. Vyazovkin, S.; Burnham, A.K.; Favergeon, L.; Koga, N.; Moukhina, E.; Pérez-Maqueda, L.A.; Sbirrazzuoli, N. ICTAC Kinetics Committee recommendations for analysis of multi-step kinetics. *Thermochim. Acta* **2020**, *689*, 178597. [[CrossRef](#)]
5. Taer, E.; Apriwandi, A.; Dalimunthe, B.K.L.; Taslim, R. A rod-like mesoporous carbon derived from agro-industrial cassava petiole waste for supercapacitor application. *J. Chem. Technol. Biot.* **2021**, *96*, 662–671. [[CrossRef](#)]
6. Silva, J.E.D.; Calixto, G.Q.; De Almeida, C.C.; Melo, D.M.A.; Melo, M.A.F.; Freitas, J.C.D.O.; Braga, R.M. Energy potential and thermogravimetric study of pyrolysis kinetics of biomass wastes. *J. Therm. Anal. Calorim.* **2019**, *137*, 1635–1643. [[CrossRef](#)]
7. Cheng, Q.; Jiang, M.; Chen, Z.; Wang, X.; Xiao, B. Pyrolysis and kinetic behavior of banana stem using thermogravimetric analysis. *Energy Source Part A* **2016**, *38*, 3383–3390. [[CrossRef](#)]
8. Kumar, A.; Mylapilli, S.V.P.; Reddy, S.N. Thermogravimetric and kinetic studies of metal (Ru/Fe) impregnated banana pseudo-stem (*Musa acuminata*). *Bioresour. Technol.* **2019**, *285*, 121318. [[CrossRef](#)] [[PubMed](#)]
9. Shakya, A.; Agarwal, T. Removal of Cr(VI) from water using pineapple peel derived biochars: Adsorption potential and re-usability assessment. *J. Mol. Liq.* **2019**, *293*, 111497. [[CrossRef](#)]
10. Sivadas, D.L.; Damodaran, A.; Raghavan, R. Microporous carbon monolith and fiber from freeze-dried banana stems for high efficiency carbon dioxide adsorption. *ACS Sustain. Chem. Eng.* **2019**, *7*, 12807–12816. [[CrossRef](#)]
11. Wang, C.; Wang, H.; Dang, B.; Wang, Z.; Shen, X.; Li, C.; Sun, Q. Ultrahigh yield of nitrogen doped porous carbon from biomass waste for supercapacitor. *Renew. Energy* **2020**, *156*, 370–376. [[CrossRef](#)]
12. Li, Y.; Zhang, D.; Zhang, Y.; He, J.; Wang, Y.; Wang, K.; Xu, Y.; Li, H.; Wang, Y. Biomass-derived microporous carbon with large micropore size for high-performance supercapacitors. *J. Power Sources* **2020**, *448*, 227396. [[CrossRef](#)]
13. Yakaboylu, G.A.; Jiang, C.; Yumak, T.; Zondlo, J.W.; Wang, J.; Sabolsky, E.M. Engineered hierarchical porous carbons for supercapacitor applications through chemical pretreatment and activation of biomass precursors. *Renew. Energy* **2021**, *163*, 276–287. [[CrossRef](#)]
14. Slopiecka, K.; Bartocci, P.; Fantozzi, F. Thermogravimetric analysis and kinetic study of poplar wood pyrolysis. *Appl. Energy* **2012**, *97*, 491–497. [[CrossRef](#)]
15. Xue, J.; Chellappa, T.; Ceylan, S.; Goldfarb, J.L. Enhancing biomass + coal Co-firing scenarios via biomass torrefaction and carbonization: Case study of avocado pit biomass and Illinois No. 6 coal. *Renew. Energy* **2018**, *122*, 152–162. [[CrossRef](#)]
16. Tahir, M.H.; Zhao, Z.; Ren, J.; Rasool, T.; Naqvi, S.R. Thermo-kinetics and gaseous product analysis of banana peel pyrolysis for its bioenergy potential. *Biomass Bioenergy* **2019**, *122*, 193–201. [[CrossRef](#)]
17. Wang, S.; Dai, G.; Yang, H.; Luo, Z. Lignocellulosic biomass pyrolysis mechanism: A state-of-the-art review. *Prog. Energy Combust.* **2017**, *62*, 33–86. [[CrossRef](#)]
18. Yeo, J.Y.; Chin, B.L.F.; Tan, J.K.; Loh, Y.S. Comparative studies on the pyrolysis of cellulose, hemicellulose, and lignin based on combined kinetics. *J. Energy Inst.* **2019**, *92*, 27–37. [[CrossRef](#)]
19. Reza, M.S.; Islam, S.N.; Afroze, S.; Bakar, M.S.A.; Taweekun, J.; Azad, A.K. Data on FTIR, TGA—DTG, DSC of invasive pennisetum purpureum grass. *Data Brief* **2020**, *30*, 105536. [[CrossRef](#)]
20. Maia, A.A.D.; de Moraes, L.C. Kinetic parameters of red pepper waste as biomass to solid biofuel. *Bioresour. Technol.* **2016**, *204*, 157–163. [[CrossRef](#)]
21. Yang, X.; Wang, X.; Zhao, B.; Li, Y. Simulation model of pyrolysis biofuel yield based on algal components and pyrolysis kinetics. *Bioenergy Res.* **2014**, *7*, 1293–1304. [[CrossRef](#)]
22. Yuan, X.; He, T.; Cao, H.; Yuan, Q. Cattle manure pyrolysis process: Kinetic and thermodynamic analysis with isoconversional methods. *Renew. Energy* **2017**, *107*, 489–496. [[CrossRef](#)]
23. Kan, T.; Strezov, V.; Evans, T.J. Lignocellulosic biomass pyrolysis: A review of product properties and effects of pyrolysis parameters. *Renew. Sustain. Energy Rev.* **2016**, *57*, 1126–1140. [[CrossRef](#)]
24. Quan, C.; Gao, N.; Song, Q. Pyrolysis of biomass components in a TGA and a fixed-bed reactor: Thermochemical behaviors, kinetics, and product characterization. *J. Anal. Appl. Pyrol.* **2016**, *121*, 84–92. [[CrossRef](#)]
25. Ahmad, M.S.; Mehmood, M.A.; Al Ayed, O.S.; Ye, G.; Luo, H.; Ibrahim, M.; Rashid, U.; Arbi Nehdi, I.; Qadir, G. Kinetic analyses and pyrolytic behavior of Para grass (*Urochloa mutica*) for its bioenergy potential. *Bioresour. Technol.* **2017**, *224*, 708–713. [[CrossRef](#)]
26. Müsellim, E.; Tahir, M.H.; Ahmad, M.S.; Ceylan, S. Thermokinetic and TG/DSC-FTIR study of pea waste biomass pyrolysis. *Appl. Therm. Eng.* **2018**, *137*, 54–61. [[CrossRef](#)]
27. Kaur, R.; Gera, P.; Jha, M.K.; Bhaskar, T. Pyrolysis kinetics and thermodynamic parameters of castor (*Ricinus communis*) residue using thermogravimetric analysis. *Bioresour. Technol.* **2018**, *250*, 422–428. [[CrossRef](#)]
28. Xu, Y.; Chen, B. Investigation of thermodynamic parameters in the pyrolysis conversion of biomass and manure to biochars using thermogravimetric analysis. *Bioresour. Technol.* **2013**, *146*, 485–493. [[CrossRef](#)]

29. Liu, Q.; Wang, S.; Zheng, Y.; Luo, Z.; Cen, K. Mechanism study of wood lignin pyrolysis by using TG–FTIR analysis. *J. Anal. Appl. Pyrol.* **2008**, *82*, 170–177. [[CrossRef](#)]
30. Wang, Z.; McDonald, A.G.; Westerhof, R.J.M.; Kersten, S.R.A.; Cuba-Torres, C.M.; Ha, S.; Pecha, B.; Garcia-Perez, M. Effect of cellulose crystallinity on the formation of a liquid intermediate and on product distribution during pyrolysis. *J. Anal. Appl. Pyrol.* **2013**, *100*, 56–66. [[CrossRef](#)]
31. Brillard, A.; Brilhac, J.F. Improvements of global models for the determination of the kinetic parameters associated to the thermal degradation of lignocellulosic materials under low heating rates. *Renew. Energy* **2020**, *146*, 1498–1509. [[CrossRef](#)]
32. Alves, J.L.F.; Da Silva, J.C.G.; Da Silva Filho, V.F.; Alves, R.F.; de Araujo Galdino, W.V.; De Sena, R.F. Kinetics and thermodynamics parameters evaluation of pyrolysis of invasive aquatic macrophytes to determine their bioenergy potentials. *Biomass Bioenergy* **2019**, *121*, 28–40. [[CrossRef](#)]
33. Du, W.; Zhang, Z.; Du, L.; Fan, X.; Shen, Z.; Ren, X.; Zhao, Y.; Wei, C.; Wei, S. Designing synthesis of porous biomass carbon from wheat straw and the functionalizing application in flexible, all-solid-state supercapacitors. *J. Alloys Compd.* **2019**, *797*, 1031–1040. [[CrossRef](#)]